CHAPTER 3

Diffusion of Nanoparticles and Biochemical Species

3.1 Introduction

In Chapters 1 and 2, we have analyzed the motion of a liquid under the form of microflow as well as under the form of microdrop (digital microfluidics). In reality the fluid we have studied in these two chapters is a buffer fluid containing the micro- and nanoparticles or macromolecules in which we are interested.

In the rest of this book, we focus on the behavior of the microparticles themselves in the buffer fluid. Different forces may act on the particles. At a microscopic scale, diffusion is always present, assuming that the particles are sufficiently small. Often, other physical phenomena superpose with diffusion. In Chapter 4, we deal with advection/diffusion problems; in Chapter 5, with biochemical reactions; in Chapter 7, with magnetic forces on magnetic beads; and in Chapter 8, with electric forces on charged and neutral microparticles. In this chapter we present the basis of the diffusion theory and the different approaches to solve diffusion problems.

First we analyze the basis of diffusion that is the random walk of particles due to the Brownian agitation of the fluid molecules. Next we introduce the diffusion equation of concentration and present some examples of applications in the biotechnology domain, and then we introduce the discrete Monte Carlo approach and some applications to the diffusion of macromolecules in the human body.

3.2 Brownian Motion

Because Brownian motion is a movement on a microscopic scale, it is no wonder that the Brownian motion was first discovered by biologists J. Ingenhousj and R. Brown [1], the latter after the observation of pollen grains floating at the surface of a drop of water.

In a gas or a liquid, there is an agitation of the molecules linked to temperature. A molecule moves in a straight line until it collides with another molecule, resulting in a change of direction. The average linear displacement between two collisions is called the mean free path.

In biotechnology, we deal with macromolecules and microparticles larger than the fluid molecules. The basic scheme of displacement is the same; the molecules of the carrier liquid collide with the macromolecules to make them perform a random walk (Figure 3.1).

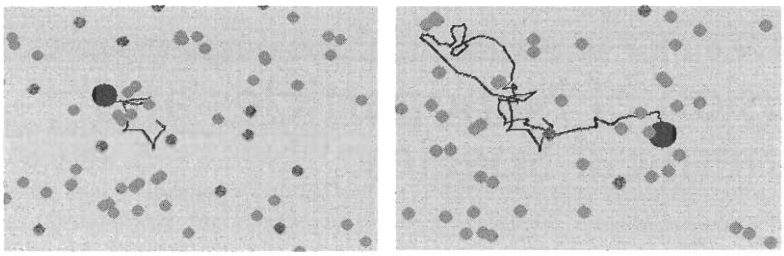

Figure 3.1 Brownian motion of a nanoparticle in a fluid at two different times. The continuous line shows the trajectory of the particle.

Brownian motion and the random walk theory is the basis of diffusion: Imagine a very small volume where the diffusing particles are initially confined. Each particle originated in this volume affects a random walk with the time, and the particles are progressively dispersed in the buffer liquid (Figure 3.2). It can be shown that the concentration follows a Gaussian profile that smears out with time.

There are two main different approaches to calculate the diffusion of these macromolecules/microparticles. The first one is the concentration approach based on the continuum hypothesis, and the second one is discrete methods where particles are followed individually.

3.3 Macroscopic Approach: Concentration

Suppose an elementary volume of liquid δV located at a coordinate (x,y,z), as shown in Figure 3.3.

The concentration c of biological species or microparticles contained in this volume at the time t is defined by the relation

$$c(x,y,z,t) = \frac{\delta m}{\delta V} \tag{3.1}$$

and a mass flux of substance through a surface is defined by [2]

$$J = \frac{\delta m}{\delta t \delta A} \tag{3.2}$$

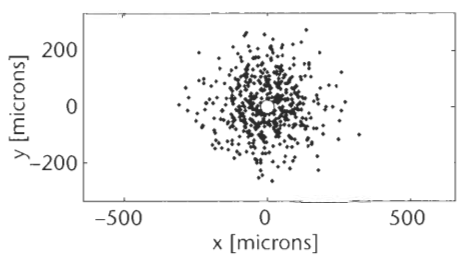

Figure 3.2 Example of diffusion from a point source. The dots are the final location of the diffusing particles at some time t.

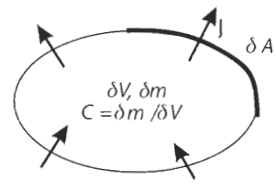

Figure 3.3 Schematization of an elementary volume with a concentration c of diffusing substance.

where the mass flux J traverses the elementary surface δA in a time interval δt. The international unit for concentration is the kilo per cubic meter (kg/m^3). However, biologists and chemists often express a concentration in mole/μL. In this case, the concentration is defined by the number of moles inside an elementary volume. The SI unit for mass flux is kg/m^2/s, and we will use also a more adapted unit (i.e., mole/μm^2/s). A fundamental law that links the mass flux to the concentration gradient is called Fick's law.

3.3.1 Fick's Law

Fick's law can be expressed as

$$J = -D\nabla c \tag{3.3}$$

where D is the diffusion constant or diffusion coefficient. The SI unit of D is m^2/s, the same as for the cinematic viscosity ν or the thermal diffusivity α. All of these quantities are coefficients in a transport equation either of concentration, velocity or enthalpy and characterized by a *flux*.

3.3.2 Concentration Equation

3.3.2.1 Differential Diffusion Equation

Using Fick's law (3.3) and evaluating the mass balance of a substance in an elementary volume of carrier liquid yields the diffusion equation

$$\frac{\partial c}{\partial t} = div(D\nabla c) + S \tag{3.4}$$

In (3.4), the term S stands for a source or sink term of concentration. For example, if there is a biochemical reaction in some part of the domain, concentration of substance may locally appear or disappear. We will come back to this point in Chapter 5.

Equation (3.4) is sometimes called Fick's second law [3]. In every subdomain where D is constant (does not depend on the spatial coordinates), (3.4) may be rewritten as

$$\frac{\partial c}{\partial t} = D\Delta c + S \tag{3.5}$$

showing that the diffusion equation is of parabolic type. Equation (3.5) is a differential equation with a solution that describes the concentration of a system as a function of time and position. The solution depends on the boundary conditions of the problem as well as on the parameter D. If the concentration c in diffusing particles or molecules is small—which is the most usual case—the diffusion coefficient D does not depend on c, and (3.5) is linear. Note that the magnitude of D is 10^{-9} m^2/s for self diffusion (diffusion of the molecules of the buffer fluid) and typically 10^{-11} m^2/s for colloidal substances.

3.3.2.2 Diffusion Coefficient

An expression of the diffusion coefficient of a particle in a carrier fluid was first obtained by Einstein. This expression may be derived by two different approaches. The first one is based on thermodynamics: The starting point is Gibbs free energy [3]. The magnitude of the driving force of diffusion is

$$F_{diffusion} = -\frac{1}{N_A}\frac{\partial \mu}{\partial x} \tag{3.6}$$

where μ is the chemical potential of the of the diffusing species and N_A is the Avogadro number. Thermodynamics show that

$$\mu = \mu_0 + RT\ln(\gamma c) \tag{3.7}$$

where γ is the activity coefficient. For dilute systems, $\gamma = 1$, and we obtain, after substitution of (3.7) in (3.6),

$$F_{diffusion} = -\frac{k_B T}{c}\frac{\partial c}{\partial x} \tag{3.8}$$

Under stationary state conditions, the diffusion force is balanced by the viscous resistance

$$F_{diffusion} = -\frac{k_B T}{c}\frac{\partial c}{\partial x} = F_{friction} = C_D v \tag{3.9}$$

where C_D is the friction factor and v is the stationary velocity. Thus,

$$v = -\frac{k_B T}{C_D c}\frac{\partial c}{\partial x} \tag{3.10}$$

If we note that the flux of material through a cross section is

$$J = vc$$

then by comparison with Fick's law, we obtain the important result

$$D = \frac{k_B T}{C_D} \tag{3.11}$$

The second approach [1] is based on Langevin's formula (similar to Newton's law, but with a complementary term for the Brownian motion)

$$m\frac{dv}{dt} = -C_D v + F(t) \tag{3.12}$$

where m is the mass of the particle, and $F(t)$ is a randomly fluctuating force representing Brownian motion. By multiplying (3.12) by x and taking the time average, we can rewrite (3.12) under the form

$$m < \frac{d}{dt}\left(x\frac{dx}{dt}\right) >= m < \left(\frac{dx}{dt}\right)^2 > -C_D < x\frac{dx}{dt} > + < xF(t) >$$

where the brackets correspond to the time averaging operation. However, because the variables x and $F(t)$ are independent,

$$< xF(t) >=< x >< F(t) >= 0$$

and the isotropic distribution of the energy yields

$$\frac{1}{2} m < \left(\frac{dx}{dt}\right)^2 >= \frac{1}{2} k_B T$$

then the Langevin equation is reduced to a differential equation

$$m < \frac{d}{dt}\left(x\frac{dx}{dt}\right) >= k_B T - C_D < x\frac{dx}{dt} > \tag{3.13}$$

The solution of (3.13) for times much larger than C_D/m is [1]

$$< x^2 >= 2\frac{k_B T}{C_D} t = 2Dt$$

and

$$D = \frac{k_B T}{C_D}$$

3.3.2.3 Anisotropic Media

In free space, diffusion is isotropic. However, in a confined space, diffusion may be anisotropic if the media containing the fluid is anisotropic [4]. Anisotropic media have different diffusion properties in different directions. Some common examples are textile fibers, polymer films, and laminated microlayers in which the molecules

have a preferential direction of orientation (Figure 3.4). It is also shown [5] that at the very vicinity of a surface, diffusion become anisotropic.

The diffusion constant D must be replace by a coefficient matrix $[D]$ where

$$[D] = \begin{bmatrix} D_{11} & D_{12} & D_{13} \\ D_{21} & D_{22} & D_{23} \\ D_{31} & D_{32} & D_{33} \end{bmatrix} \tag{3.14}$$

The mass flux is then anisotropic and Fick's law can be written under the form [4]

$$\begin{Bmatrix} J_x \\ J_y \\ J_z \end{Bmatrix} = -[D]\nabla c \tag{3.15}$$

Finally the diffusion equation is

$$\frac{\partial c}{\partial t} = D_{11}\frac{\partial^2 c}{\partial x^2} + D_{22}\frac{\partial^2 c}{\partial y^2} + D_{33}\frac{\partial^2 C}{\partial z^2} + \left(D_{23} + D_{32}\right)\frac{\partial c}{\partial y \partial z}$$
$$+\left(D_{31} + D_{13}\right)\frac{\partial c}{\partial z \partial x} + \left(D_{12} + D_{21}\right)\frac{\partial c}{\partial x \partial y}$$

if the Ds are taken constant. We may rotate the axis in order to transform the rectangular coordinates (x,y,z) into the rectangular coordinates (ξ, η, ζ) characterizing the principal axes of diffusion, and the preceding equation becomes

$$\frac{\partial c}{\partial t} = D_1\frac{\partial^2 c}{\partial \xi^2} + D_2\frac{\partial^2 c}{\partial \eta^2} + D_3\frac{\partial^2 c}{\partial \zeta^2} \tag{3.16}$$

It is possible to make the further transformation

$$\xi_1 = \xi\sqrt{\frac{D}{D_1}}, \eta_1 = \eta\sqrt{\frac{D}{D_2}}, \zeta_1 = \zeta\sqrt{\frac{D}{D_3}}$$

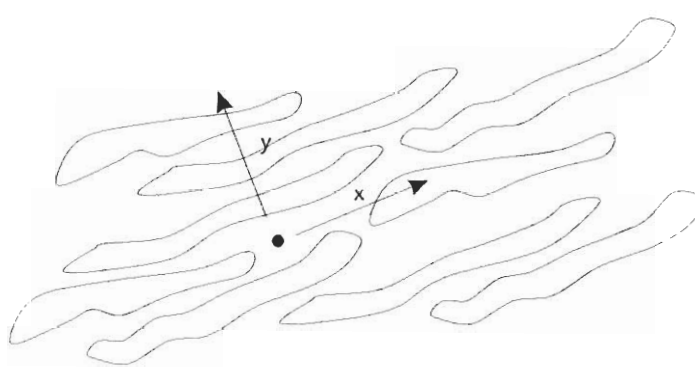

Figure 3.4 Sketch of an anisotropic media. The preferred direction of diffusion is the x-direction.

where D is arbitrary, to obtain

$$\frac{\partial c}{\partial t} = D\left[\frac{\partial^2 c}{\partial \xi_1^2} + \frac{\partial^2 c}{\partial \eta_1^2} + \frac{\partial^2 c}{\partial \zeta_1^2}\right] \tag{3.17}$$

Equation (3.17) has an isotropic value for the diffusion constant D to the price of a rotation plus a homothetic transformation of the axes. In Section 3.3.8, for some reasons that we explain, we proceed in an opposite way: We transform a very elongated (anisotropic) computational domain into a more regular domain. This transformation requires that the initially isotropic diffusion coefficient be changed into an anisotropic diffusion matrix.

3.3.3 Spreading from a Point Source—1D Case

We analyze here the diffusion of a substance (tracers or nanoparticles) in a one-dimensional geometry. Suppose that a very small spot of concentration of tracer particles has been initially placed in a rectangular capillary of very small cross section (Figure 3.5).

In such a case, the diffusion may be considered one-dimensional and depends one two variables: the time t and the axial coordinate x. The initial condition may be approximated by:

$$c(x,t_0) = c_0\delta(x) \tag{3.18}$$

where $\delta(x)$ is the Dirac function. With such an initial condition, the solution to (3.5) is

$$c(x,t) - \frac{c_0}{\sqrt{4\pi Dt}} e^{-\frac{x^2}{4Dt}} \tag{3.19}$$

The solution (3.19) shows that the distribution profile of concentration in tracers is Gaussian in x. In Figure 3.6, we have plotted the solution of (3.19) with scaling c/c_0 for $D = 10^{-10}$ m^2/s at three different times (0.2, 1, and 10 seconds).

Note that the characteristic nondimensional group $\frac{x^2}{4Dt}$ appears in the solution (3.19) of (3.5). This group represents in fact a characteristic diffusion length. The characteristic diffusion length may be defined by

$$x_c \approx \sqrt{4Dt} \tag{3.20}$$

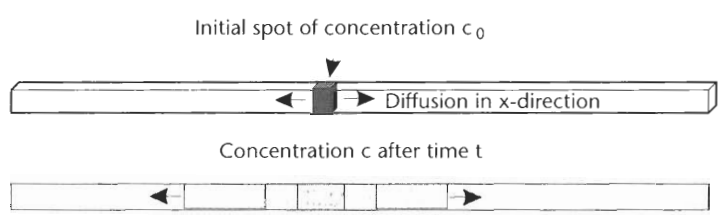

Figure 3.5 Schematic view of the diffusion of tracers in a one-dimensional geometry.

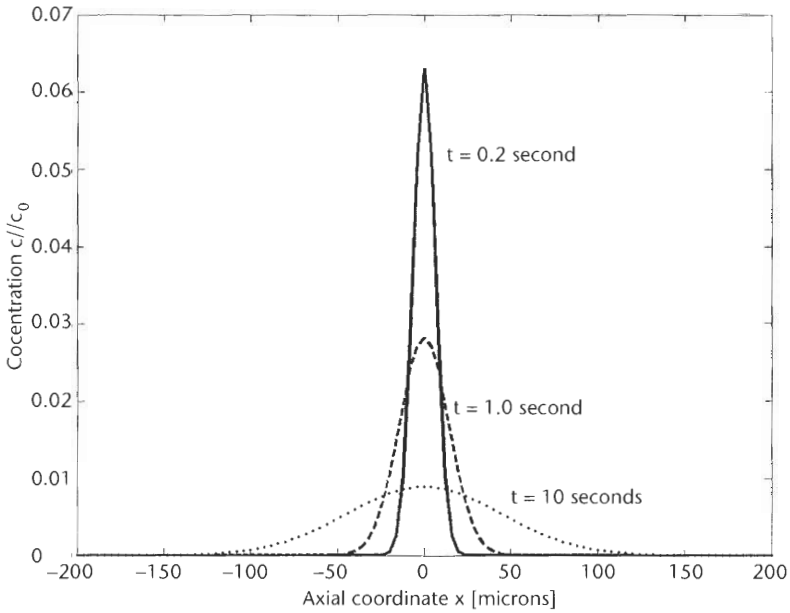

Figure 3.6 Gaussian profiles of diffusion from a point source according to (3.19).

In the preceding example, one finds by using (3.20): $x_c(t = 0.2) \sim 10\ \mu$m; $x_c(t = 1.0) \sim 20\ \mu$m; and $x_c(t = 10) \sim 60\ \mu$m.

3.3.4 The Ilkovic's Solution for a Semi-Infinite Space

It is seldom that the diffusion equation (3.4) can be solved analytically. There are some one-dimensional cases where an analytical solution may be found (we have seen one in the preceding section); but usually, as soon as the geometry of the diffusion problem is two-dimensional, or if the one-dimensional problem presents complex boundary conditions, the use of a numerical approach is required to solve the diffusion equation (3.4). We expose here the analytical solution of the diffusion equation in the simple case of diffusion of species in a half space.

Suppose a half-space with an initial concentration of c_0. Suppose also that any microparticle or macromolecule that contacts the solid wall limiting the half-space domain is immediately immobilized. Then the concentration at the wall is zero at any time.

The solution for the concentration equation is then

$$c = c_0 erf\left(\frac{x}{\sqrt{4Dt}}\right) \tag{3.21}$$

where x is the distance from the wall, and the error function erf is defined by

$$erf(x) = \frac{2}{\sqrt{\pi}} \int_0^x e^{-u^2}\, du$$

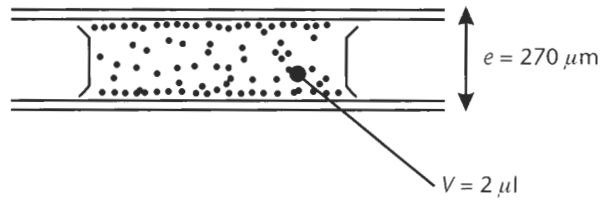

Figure 3.7 Schema of the drop and the two glass plates.

This function has the following characteristic values: $erf(0) = 0$ and $erf(\infty) = 1$ and its derivative is $\frac{d(erf)}{dx} = \frac{2}{\sqrt{\pi}} e^{-x^2}$. Thus, the space derivative of (3.21) is

$$\frac{\partial c}{\partial x} = c_0 \frac{2}{\sqrt{\pi}} e^{-\frac{x^2}{4Dt}} \frac{1}{\sqrt{4Dt}}$$

With this in mind, the mass flux per surface unit, given by Fick's law, may be written under the form

$$\vec{J} = -D\nabla c_{|wall} = -D\frac{\partial c}{\partial x}_{|x=0} = -Dc_0 \frac{2}{\sqrt{\pi}} \frac{1}{\sqrt{4Dt}} \hat{i} = -c_0 \sqrt{\frac{D}{\pi t}} \hat{i} \tag{3.22}$$

where $\hat{i}$ is the unit vector perpendicular to the wall. This latter relation is called the Ilkovic's solution to the diffusion problem. It shows that the mass flux is proportional to the concentration far from the wall and to the square root of the diffusion coefficient. Strictly, from (3.22), the initial mass flux is infinite. In fact, on a practical point of view, such a situation is not possible: There is always a transition time during which the fluid with the concentration c_0 is brought in contact with the wall, and the initial time for diffusion is always approximate.

3.3.5 Example of Diffusion Between Two Plates

In this section, we show the limitation of Ilkovic's solution for the problem of diffusion between two plates. Suppose that we insert a small volume of liquid ($V = 2\ \mu l$) between two parallel horizontal glass plates (Figure 3.7) separated by a distance of 270 μm. The liquid contains nanoparticles (hydrodynamic diameter $D_H = 100$ nm, diffusion coefficient $D = 0.21 \cdot 10^{-11}$ m^2/s) in concentration c_0.

At the beginning, the particles are uniformly dispersed in the liquid at rest; progressively, the particles closer to the walls are immobilized by contact with the walls under the action of the Brownian motion, and a concentration depletion progresses from the walls toward the drop center.

It is possible to count the number of particles immobilized at any time on the photographs of the upper plate taken under the microscope (Figure 3.8). It may be shown that the particle size is so small that sedimentation can be completely neglected, and we assume that there is statistically the same number of particles immobilized on the upper and lower plate.

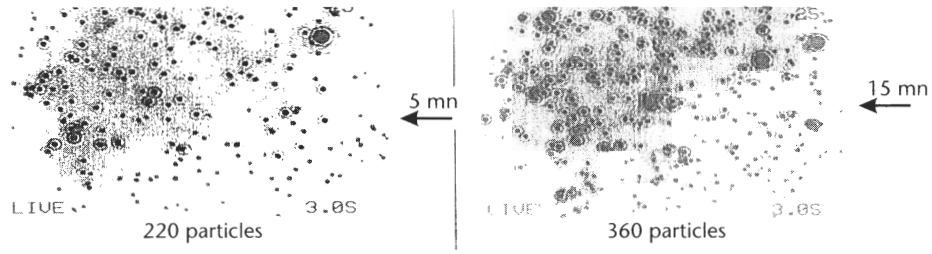

Figure 3.8 Photographs of the upper plate taken under the microscope after 5 mn and 15 mn. (Courtesy of D. Marsi, CEA/LETI.)

Assuming that the drop is cylindrical (which is the equilibrium shape—see Chapter 2), diffusion process is governed by the two-dimensional axisymmetrical equation

$$\frac{\partial c}{\partial t} = div(D\ grad\ c) = D\left(\frac{1}{r}\frac{\partial c}{\partial r} + \frac{\partial^2 c}{\partial r^2} + \frac{\partial^2 c}{\partial z^2}\right) \tag{3.23}$$

In this particular case, we can express the concentration in particles per unit volume, and the mass flux at the wall J is then expressed in particles per seconds per unit surface. The mass flux at each wall (defined by $z = 0$ and $z = e$) is given by Fick's law

$$|J| = |J_{upper}| + |J_{lower}| = -D\frac{\partial c}{\partial z}\bigg|_{z=e} + D\frac{\partial c}{\partial z}\bigg|_{z=0} \tag{3.24}$$

If we suppose that the radial dimension R of the drop is large in front of the distance between the plates e, we can approach (3.23) by the one-dimensional equation

$$\frac{\partial c}{\partial t} = div(D\ grad\ c) = D\frac{\partial^2 c}{\partial z^2} \tag{3.25}$$

A first approach to the problem consists of solving (3.25) for times less than $\tau = \dfrac{\left(\frac{e}{2}\right)^2}{4D}$. For these times, the depletion of concentration has not reached the center plane of the drop. The problem is then similar to that of Ilkovic for each plate, and the solution of (3.24) is

$$J = 2c_0\sqrt{\frac{D}{\pi t}} \tag{3.26}$$

This solution breaks down when the concentration at the center plane starts decreasing from its initial value c_0. So when the time is larger than $\tau = \dfrac{\left(\frac{e}{2}\right)^2}{4D}$,

Ilkovic's solution is no more valid. In Figure 3.9, we compare the experimental results (dots) to the Ilkovic's solution and to the results of a simple one-dimensional numerical scheme (finite differences method).

Vertical concentration profiles at different times—obtained by the numerical method—are plotted in Figure 3.10. At the beginning, the profile is still flat at the center with a concentration c_0. At times t larger than τ, the concentration at the center plane decreases below the value c_0.

3.3.6 Radial Diffusion

In the case of a purely radial diffusion from a source point or a central sphere (Figure 3.11), the diffusion equation is

$$\frac{\partial c}{\partial t} = D\left[\frac{\partial^2 c}{\partial r^2} + \frac{2}{r}\frac{\partial c}{\partial r}\right] \tag{3.27}$$

On putting [4]

$$u = cr \tag{3.28}$$

Equation (3.27) becomes

$$\frac{\partial u}{\partial t} = D\frac{\partial^2 u}{\partial r^2} \tag{3.29}$$

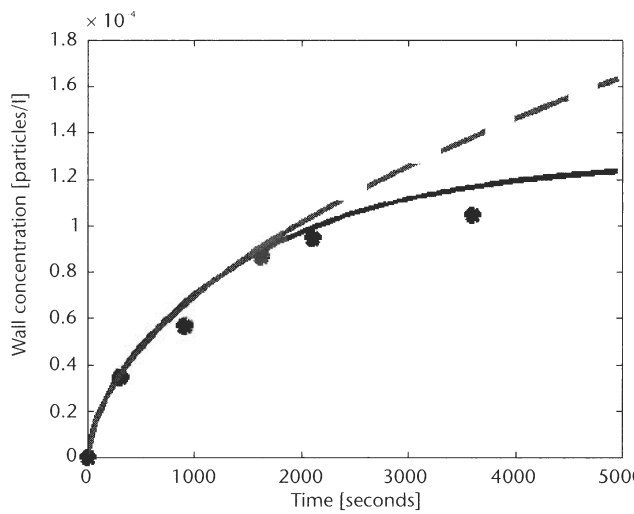

Figure 3.9 Wall concentration of immobilized nanoparticles (particles/μm^2) as a function of time. Comparison between measurements (dots), Ilkovic's solution, and numerical results. Before $t < \tau = \frac{\left(\frac{e}{2}\right)^2}{4D} = 2166s$, all of the results are close together. After the time τ, the Ilkovic solution departs from the experimental results, whereas the numerical results still agree with the experimental results.

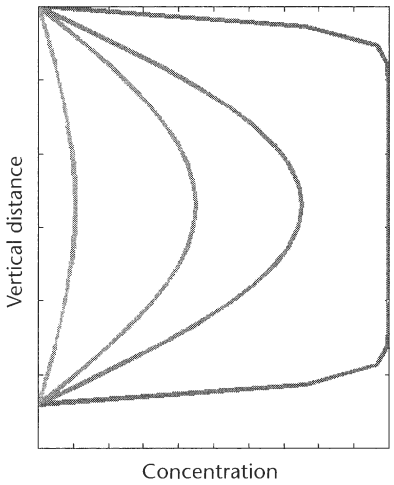

Figure 3.10 Vertical profiles of concentration c/c_0 versus time.

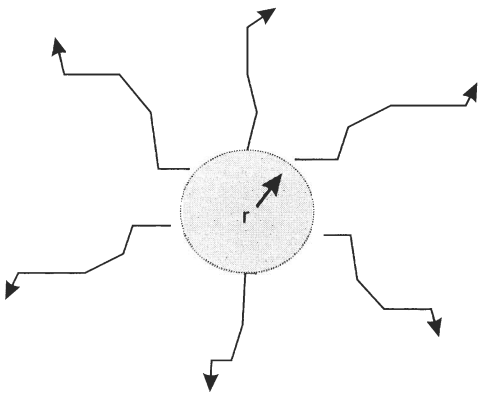

Figure 3.11 Radial diffusion from an initial spherical volume.

This equation is formally the same as the one-dimensional diffusion equation and can be solved by using the same methods.

3.3.6.1 Steady State Solution

In the case of a steady state problem, (3.29) becomes

$$\frac{d}{dr}\left(r^2 \frac{dc}{dr}\right) = 0 \tag{3.30}$$

of which the general solution is

$$c = \frac{A}{r} + B \tag{3.31}$$

where A and B are constants to be determined from the boundary conditions.

3.3.6.2 Transient Solution

In the case of a spherical surface with a constant concentration $c_1(r = a)$ and an external concentration $c_0(r > a)$, the solution is derived directly from the one-dimensional Ilkovic's solution

$$\frac{c - c_0}{c_1 - c_0} = \frac{a}{r}\left(1 - erf\frac{r - a}{\sqrt{4Dt}}\right) \tag{3.32}$$

3.3.7 Diffusion Inside a Microchamber

The standard biodiagnostic procedure for DNA recognition is the polymerase chain reaction (PCR). However, there have been recently developments of new microdevices using direct detection of DNA strands by fluorescence (Figure 3.12). The principle is to bring the DNA strands inside the microchamber (e.g., using magnetic particles) and then let them diffuse so that the DNA strands can hybridize on a labeled surface. Because the system must be very sensitive and work with very few DNA strands, it is important to stop any back diffusion toward the inlet channel.

A very simple analysis of the diffusion inside the microchamber may be done by considering the diffusion equation in the two-dimensional geometry defined by Figure 3.13 and using standard numerical techniques. The results presented in Figure 3.14 have been obtained by discretization of the diffusion equation by using a Crank-Nicholson formulation [6]. The two-dimensional diffusion equation may be written under the form

$$\begin{aligned}\frac{c_{i,j}^{n+1} - c_{i,j}^{n}}{\Delta t} &= \frac{D}{2}\left[\frac{c_{i+1,j}^{n+1} - 2c_{i,j}^{n+1} + c_{i-1,j}^{n+1}}{(\Delta x)^2} + \frac{c_{i,j+1}^{n+1} - 2c_{i,j}^{n+1} + c_{i,j-1}^{n-1}}{(\Delta y)^2}\right] \\ &+ \frac{D}{2}\left[\frac{c_{i+1,j}^{n} - 2c_{i,j}^{n} + c_{i-1,j}^{n}}{(\Delta x)^2} + \frac{c_{i,j+1}^{n} - 2c_{i,j}^{n} + c_{i,j-1}^{n}}{(\Delta y)^2}\right]\end{aligned} \tag{3.33}$$

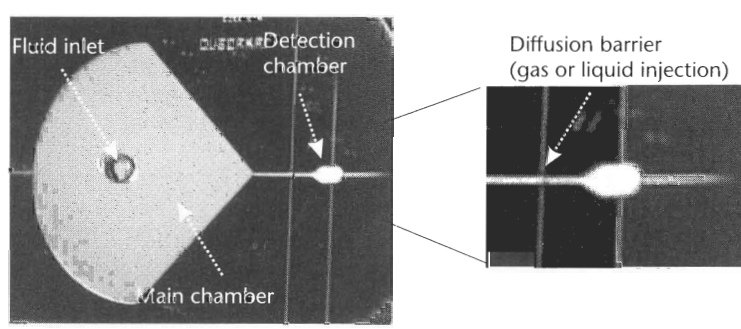

Figure 3.12 Biodiagnostic detection device. Left: view of the main and detection microchambers. Right: close up on the detection chamber. (Courtesy of F. Ginot and R. Campagnolo, LETI/BioMérieux.)

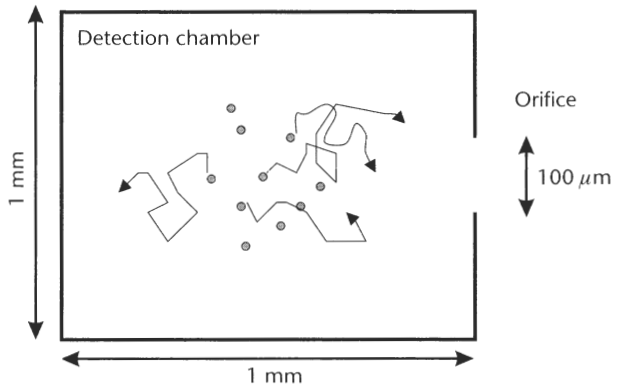

Figure 3.13 Schematic view of the computation domain.

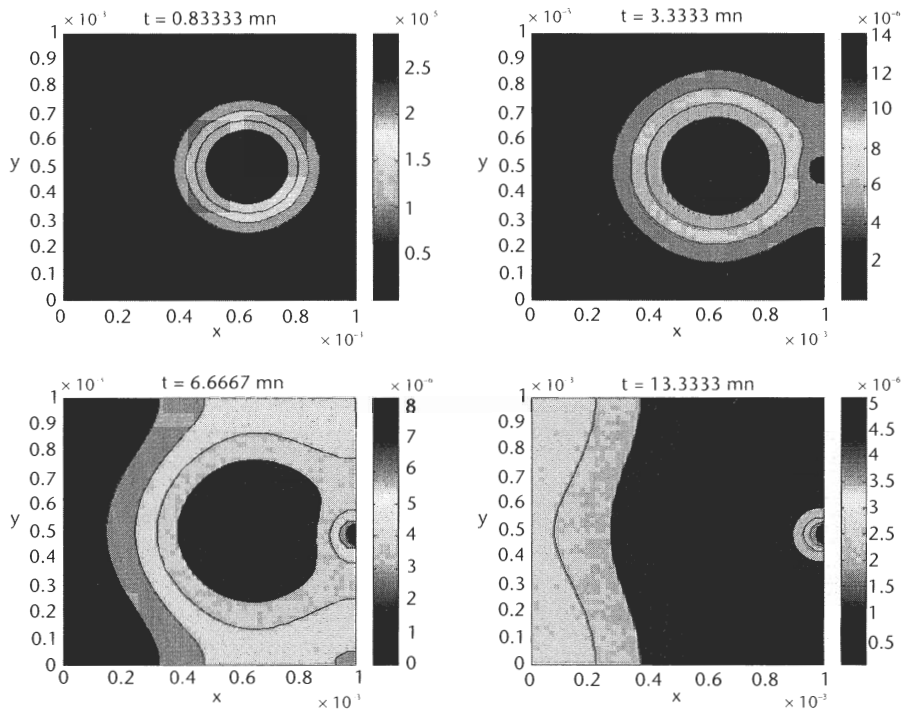

Figure 3.14 Diffusion of macromolecules initially concentrated in the middle of the detection microchamber (the macromolecules are released from the aggregate of magnetic beads). The right side of the chamber is considered an exit toward the inlet channel.

where i and j are the indices corresponding to the space location, and n is the time index. Equation (3.33) can be written in a matrix form and inverted to obtain the solution for the concentration at each time step t_n at every point of the computational grid.

An analysis of the results shows that it is necessary to stop back diffusion inside the inlet channel. This is done by injecting a gas in secondary reservoirs (by thermal expansion for example) (Figure 3.15).

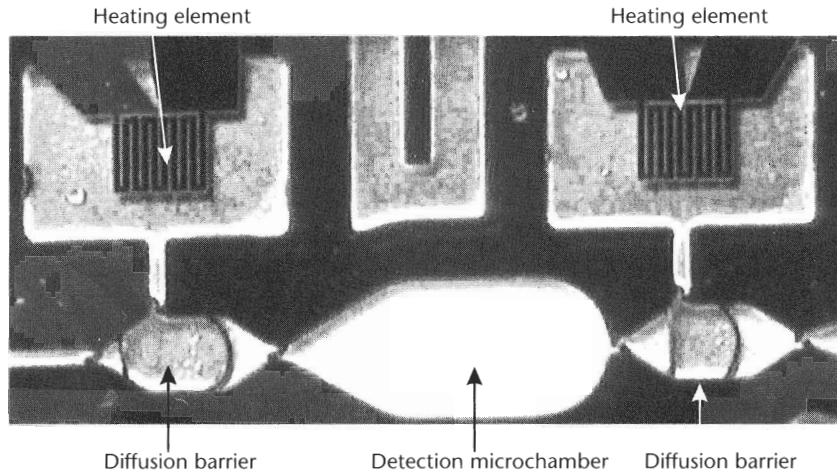

Figure 3.15 Enlarged view of the detection chamber and diffusion blocking reservoirs. (Courtesy of N. Sarrut, CEA/LETI.)

3.3.8 Diffusion Inside a Capillary: The Example of Simultaneous PCRs

3.3.8.1 Introduction

Biorecognition and detection of DNA by PCR is still the most often used procedure. In order to parallelize PCR reactions—and other similar biological analyses—it has been thought to perform these operations at the same time at different locations in a capillary tube [7]. In this example of the simultaneous PCRs, the biological sample to be analyzed is brought into the tube under the action of capillary forces (or by pipetting). At the solid wall, at different locations, different primers (reverse and forward) have been immobilized (Figure 3.16).

When the liquid has filled the tube and is at rest, the primers are released by optical methods (insolation) and then diffuse locally inside the tube (Figure 3.17). The presence of both reverse and forward primers is necessary for PCR amplification. In the regions of the tube where a sequence of the DNA contained in the liquid is corresponding to a type of primer, DNA amplification occurs, and detection is made by fluorescence methods.

Within the time frame of the PCR cycles for amplification, the primers should not diffuse to the next region in a substantial way (Figure 3.18). If they do, detection would be inaccurate. Thus, it has been planned to introduce neutral gaps between

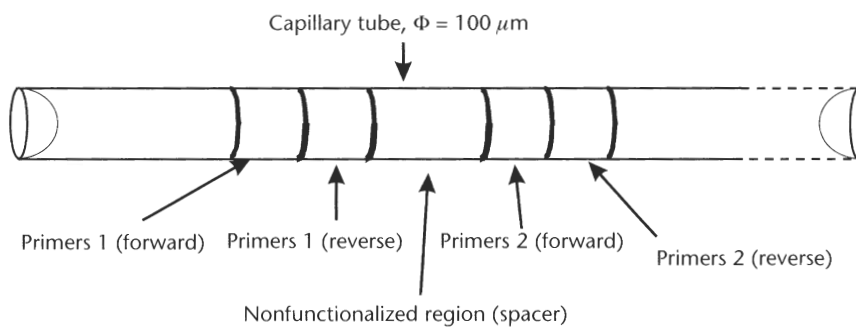

Figure 3.16 Schematic view of the capillary with the different labeled regions.

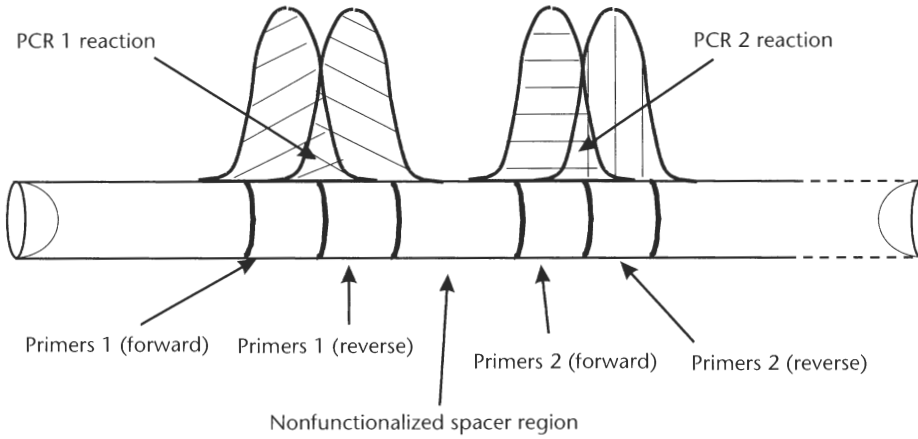

Figure 3.17 Schematic view of the primers concentration and the PCR reaction regions (drawing not to scale).

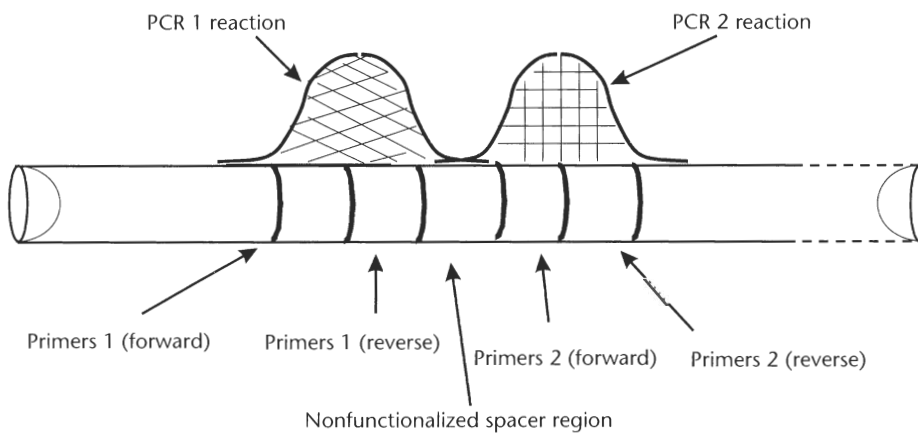

Figure 3.18 Schematic view of the concentration profile of the different PCR reaction products.

the primers regions so that there is no diffusion of primers between two regions. However, the aim is a compact microsystem, and these gaps should be reduced as much as possible. The problem consists of calculating the primers diffusion inside the tube and determining their concentration as a function of time.

In the following sections, we present two approaches to calculate the diffusion inside the capillary. The first one is an analytical approach, based on the simplification that the concentration in primers—after a few seconds—is uniform in a cross section of the tube. The second approach consists of numerically solving the diffusion equation after it has been rendered nondimensional. The advantage of this second solution is that it gives an insight on diffusion barrier.

3.3.8.2 Analytical Model for Diffusion Inside a Tube

First, taking into account that the ratio L/R between the tube length and the tube radius is large, we show that we can assume the concentration in primers uniform in

any cross section in a very short time after their release from the wall. A characteristic diffusion time for a primer to diffuse on the length R is

$$\tau \approx \frac{R^2}{4D} \tag{3.34}$$

Primers have a diffusion coefficient of the order $D = 10^{-10}$ m^2/s, and suppose that the radius of the tube is $R = 50\ \mu$m. The characteristic time is then $\tau = 6$ seconds. During the time τ, axial diffusion is not significant, as we can show by using a very simple Monte Carlo approach (Figure 3.19).

So we may assume a uniform concentration in primers in any annular volume delimited by the initial functionalized regions (volume $V = \pi R^2 a$, where a is the length of a region).

After the time τ, the primers are homogeneously scattered in the different annular volumes. The second step consists of calculating the concentration of the primers as a one-dimensional diffusion phenomenon. For each primer i, we have

$$\frac{\partial c_i}{\partial t} = D_i \frac{\partial^2 c_i}{\partial z^2} \tag{3.35}$$

An analytical solution to (3.35) is given by the following combination of error functions [4]:

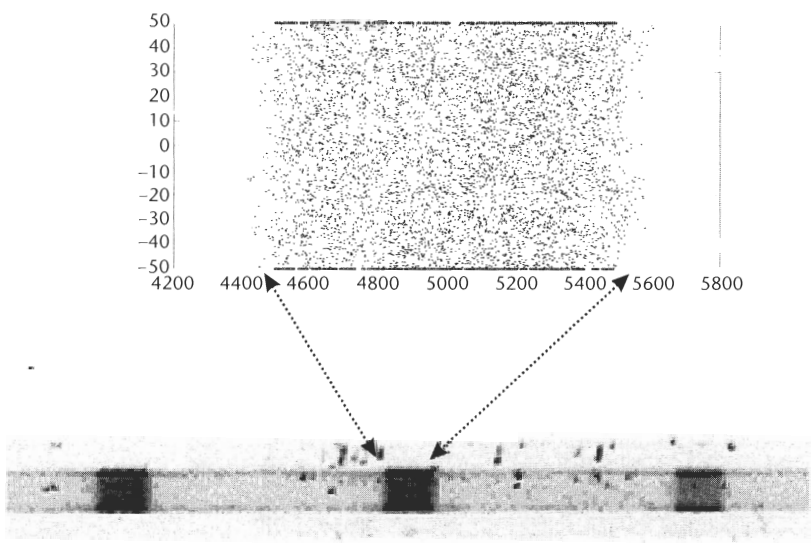

Figure 3.19 Diffusion of primers from the wall after 6 seconds (obtained by a Monte Carlo simulation). The starting location of the primers has been randomly chosen on the walls. The diffusion outside the annular volume is still negligible at that time. Bottom: experimental results. (Courtesy of CEA/LETI.)

$$c_i = \frac{1}{2} c_{0,i} \left[erf\left(\frac{a_i - z}{2\sqrt{D_i t}} \right) + erf\left(\frac{a_i + z}{2\sqrt{D_i t}} \right) \right] \tag{3.36}$$

In Figure 3.20, concentration profiles of two neighboring primers with different coefficients of diffusion have been plotted. It is immediately seen that a spacer gap must be introduced between the two regions to prevent cross mixing.

The advantage of the analytical solution is that we can produce an expression of the required spacing between the functionalized regions. Suppose that the concentration in primers i in region $i + 1$ should not be larger than a threshold concentration c_{max}, at a time t_f defined by the kinetics of amplification; then the minimum distance z_{min} between the two regions i and $i + 1$ is given by the implicit relation

$$\frac{2c_{max}}{c_{0,i}} = \left[erf\left(\frac{a_i - z_{min}}{2\sqrt{D_i t_f}} \right) + erf\left(\frac{a_i + z_{min}}{2\sqrt{D_i t_f}} \right) \right] \tag{3.37}$$

The solution of (3.37) requires us to find the zero of a function, which is a standard procedure to most mathematical software.

3.3.8.3 Dimensional Analysis

This analytical method is a fast and simple way to find an approximate solution to the problem. However, a dimensional analysis reveals more of the physics of axial diffusion and will be the basis for a numerical approach. Start from the axisymmetrical diffusion equation for each primer

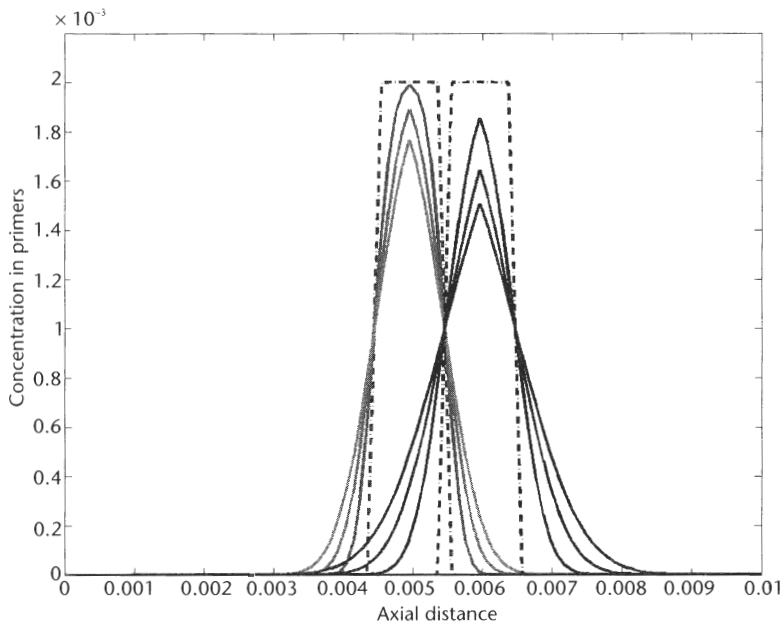

Figure 3.20 Concentration plot of the solution of (3.36) at different times. The two primers have different diffusion coefficients.

$$\frac{\partial c}{\partial t} = div(D\ grad\ c) = D\left(\frac{1}{r}\frac{\partial c}{\partial r} + \frac{\partial^2 c}{\partial r^2} + \frac{\partial^2 c}{\partial z^2}\right) \tag{3.38}$$

and note that the capillary length L is very large before the capillary radius R. If we want to set up a numerical calculation, we have to deal with a computational domain with a very large aspect ratio L/R. We can introduce the new variables

$$z^* = \frac{z}{L}, r^* = \frac{r}{R} \tag{3.39}$$

so that the transformed computational domain is defined by $L^* = 1$, $R^* = 1$. Let's introduce the other nondimensional variables

$$c^* = \frac{c}{c_0}, t^* = \frac{t}{\frac{RL}{D}} \tag{3.40}$$

It is straightforward to see that the nondimensional diffusion equation is

$$\frac{\partial c^*}{\partial t^*} = \frac{L}{R}\left(\frac{1}{r^*}\frac{\partial c^*}{\partial r^*} + \frac{\partial^2 c^*}{\partial r^{*2}}\right) + \frac{R}{L}\frac{\partial^2 c^*}{\partial z^{*2}} \tag{3.41}$$

This equation is an axisymmetrical diffusion equation with the anisotropic diffusion coefficients

$$D^*_z = \frac{R}{L}, D^*_r = \frac{L}{R} \tag{3.42}$$

In order to compensate for the change in geometry, the diffusion coefficients are now strongly anisotropic; the equivalent diffusion coefficient in the direction r is large, whereas that in the direction z is small. The ratio between the r and z diffusion coefficient is

$$\frac{D^*_r}{D^*_z} = \frac{L^2}{R^2} >> 1$$

Note that (3.41) verifies Buckingham's Pi theorem [8]. There are four independent parameters in (3.38): c_0, L, R, and D. These parameters depend on three different units: kilos or moles (if we count the concentration in kilos or moles), meters, and seconds. According to Buckingham's theorem, there should be $4 - 3 = 1$ dimensionless parameter in the nondimensional equation. This parameter is evidently L/R.

3.3.8.4 Numerical Solution

Equation (3.41) may be solved by using a standard finite element method. The computational domain is defined by $r^* \in \{0,1\}, z^* \in \{0,1\}$. At the wall, the condition of

impermeability yields $\frac{\partial c^*}{\partial r^*}\Big|_{r^*=1} = \frac{\partial c}{\partial r}\Big|_{r=R} = 0$. An initial condition $c^*_0 = 1$ is imposed in a very small volume at the periphery of the tube. Concentration contours obtained at two different times are shown in Figure 3.21.

Note that the nondimensional calculations results have to be back transformed into dimensional values. It is a straightforward process if we use (3.39) and (3.40), and if we note that the initial concentration c_0 is obtained by converting the surface concentration in immobilized primers into a volume concentration.

3.3.8.5 Diffusion Barriers

It can be checked that the analytical and numerical results agree (Figure 3.22). Most of the time, analytical results when sufficiently accurate should be preferred. However, in the present case, the numerical approach—although more complex to set up—is more powerful. For example, it is possible to investigate whether axial diffusion inside the tube can be reduced. Although this problem is discussed in Chapter 5 (biochemical reactions), it is a diffusion barrier problem and we will mention it here. We found that if the gap between the annular regions initially labeled with the primers were adequately functionalized, the recapture of the

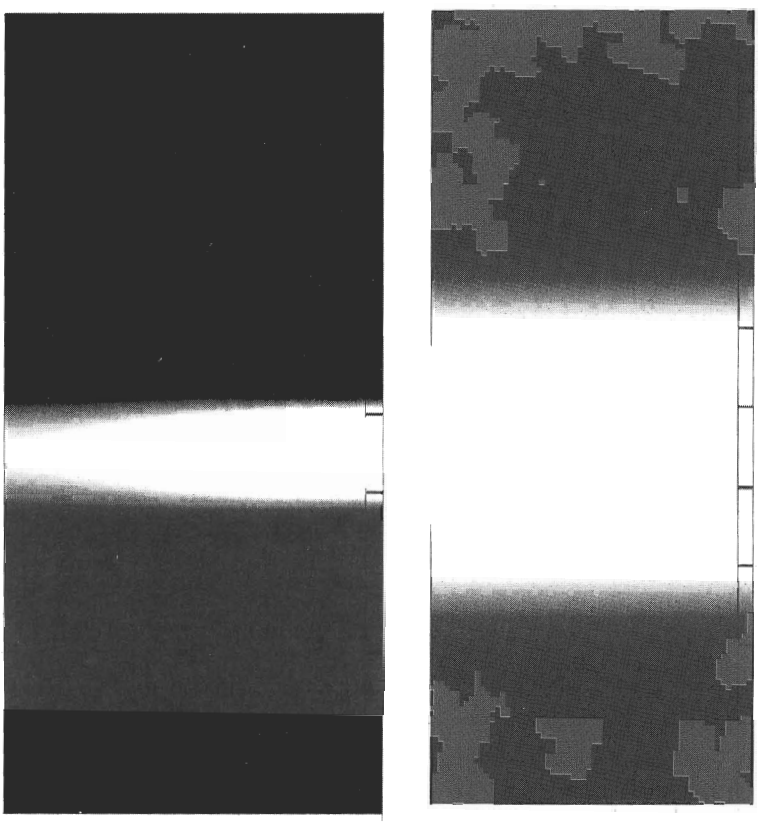

Figure 3.21 Concentration contours at two different times calculated with the numerical software FEMLAB [9], showing the same behavior as the analytical approach.

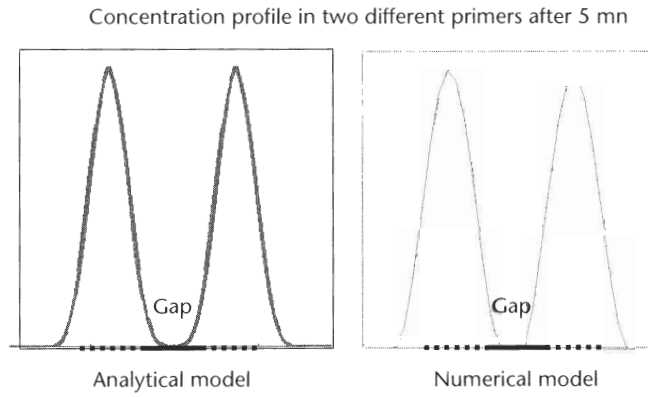

Figure 3.22 Comparison of concentration profiles between analytical and numerical models after the same time interval.

primers during diffusion would limit the axial diffusion. In Figure 3.23, we compare the axial diffusion of primers for a simple gap and a labeled gap.

3.3.9 Particle Size Limit: Diffusion or Sedimentation

The following question stems out of an inspection of (3.5): Does gravity force—which is not present in the equation—affect the diffusion of the microparticles? In other words, is the apparent weight of the particles negligible? One conceives easily that if the particles are small enough they will not sediment, and they will diffuse in the available volume; if they are sufficiently large, they will sediment despite the molecular agitation [3]. We derive here a criterion to estimate the sedimentation of the microparticles and to decide if the diffusion equation is valid.

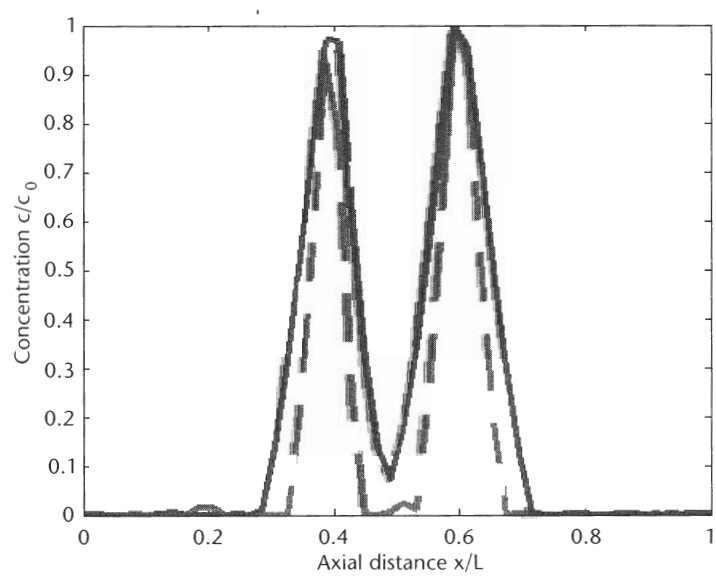

Figure 3.23 Comparison of the concentration profiles between a labeled (dotted line) and a nonlabeled (continuous line) gap. Axial diffusion is remarkably reduced if the gaps are labeled.

The settling velocity is defined as the uniform vertical velocity of a particle in a liquid at rest. The settling velocity can be calculated by writing the balance between gravitational force and hydrodynamic drag. If C_D be the friction factor (hydrodynamic drag coefficient), C_D is defined by

$$C_D = 6\pi\eta R_H \tag{3.43}$$

Then, the hydrodynamic drag force on the particle is

$$F_{friction} = C_D v = 6\pi\eta R_H v \tag{3.44}$$

and the settling velocity V_S is obtained by the force balance

$$C_D V_S = \Delta\rho g Vol_p \tag{3.45}$$

where $\Delta\rho$ is the buoyancy density (difference between the volumic mass of particle and liquid), η is the dynamic viscosity of the fluid, and g is the gravity acceleration (9.8 m/s^2). For a spherical particle, the sedimentation velocity is given by

$$V_S = \frac{2}{9}\frac{\Delta\rho g R^2}{\eta} \tag{3.46}$$

Suppose now that a typical dimension of the problem is d. For example, the vertical dimension of a biodiagnostic microchamber is of the order of $d = 50\,\mu$m. Let us compute the times τ_1 and τ_2 for the particle to move on the distance d by sedimentation and Brownian motion

$$\tau_1 = \frac{d}{V_S}$$

and

$$\tau_2 \approx \frac{d^2}{4D}$$

then, the ratio $\beta = \tau_1/\tau_2$ is

$$\beta = \frac{\tau_1}{\tau_2} \approx \frac{d}{V_S}\frac{4D}{d^2} = 4\frac{k_B T}{\Delta\rho g d Vol_p} = 4\frac{k_B T}{\Delta m g}\frac{1}{d} \tag{3.47}$$

If we introduce the characteristic Boltzmann length scale L [5], (3.47) becomes

$$\beta = 4\frac{L}{d}$$

The ratio (3.47) is an energy ratio between the energy of the Brownian motion and the potential energy of the particle. If $\beta << 1$, sedimentation dominates, and the particles will descend with the settling velocity. As a general rule, particles larger

than 1 μm tend to be affected by sedimentation. For example, cells usually sediment because their size is larger than 10 μm. A more detailed analysis may be found in [3].

The preceding analysis shows that it is very important not to let the particles aggregate. If so, the Brownian motion will cease, and the aggregate will sediment. This is why surfactants or poly-ethylene-glycol (PEG) [10] are usually added to buffer liquids.

3.4 Microscopic (Discrete) Approach

In the preceding sections, we have followed an approach based on the continuum: this approach assumes that in every elementary volume of liquid there are a number of microparticles sufficiently important to define a concentration. This approach is very convenient because it introduces a PDE that can be solved by ordinary discretization techniques, like the finite element method or the finite volume method. However, very complex geometries of the diffusion domain may not be easily treated with such methods.

We present here another approach that is very useful when dealing with microscopic scales. Contrary to the preceding continuum approach, this approach is discrete, meaning that the displacement of every particle is calculated. This approach is well adapted to complex geometrical domains and small number of particles.

3.4.1 Monte Carlo Method

The Monte Carlo method is based on the mimicking of the random walk of particles. Because the mean free path is very short, it is possible without changing the statistical randomness to allow for longer linear displacement steps, at the condition that they remain small compared to the free space defined by the surrounding geometry.

3.4.1.1 Two-Dimensional Case

In the two-dimensional case, a particle moves in a time step Δt from the location (x, y) to the location $(x + \Delta x, y + \Delta y)$, where the space increments are defined by

$$\begin{aligned} \Delta x &= \sqrt{4D\Delta t}\cos(\alpha) \\ \Delta y &= \sqrt{4D\Delta t}\sin(\alpha) \\ \alpha &= random(0,2\pi) \end{aligned} \tag{3.48}$$

In (3.48) the function "random" is a choice of uniformly distributed random numbers in the interval $[0, 2\pi]$. The validity of the method depends on the quality of randomness of the angle α. In the following we have used the MATLAB command "rand" [11]. The length of the displacement has been scaled by the real diffusion-length scale.

Example of Random Walk from a Source Point

We show here two examples of random walk calculations. The first case is the two-dimensional diffusion from a source point (Figure 3.24).

Using the algorithm defined by (3.48), we find the pictures of Figure 3.25. Diffusion is isotropic around the initial spot and has a Gaussian shape along a radius.

In Figure 3.26, it can be verified that the average square distance is related to time by the relation

$$< d^2 >= 4Dt$$

Example of Random Walk in a Microchannel

The same algorithm can be applied to the case of a microchannel. The results are shown in Figure 3.27. In this case also, the particle distribution follows a Gaussian profile.

3.4.1.2 Three-Dimensional Case

In the three-dimensional case, a particle moves in a time step Δt from the location (x, y, z) to the location $(x + \Delta x, y + \Delta y, z + \Delta z)$. The random walk algorithm is the following

$$\begin{aligned} \Delta x &= \sqrt{4Ddt}\cos(\alpha)\sin(\beta) \\ \Delta y &= \sqrt{4Ddt}\sin(\alpha)\sin(\beta) \\ \Delta z &= \sqrt{4Ddt}\cos(\beta) \\ \alpha &= random(0,2\pi) \\ \beta &= \arccos\left(1-2\ random(0,1)\right) \end{aligned} \tag{3.49}$$

The angles α and β are defined in Figure 3.28. Note the definition of the angle β in (3.49). If we had taken simply β = random $(0, 2\pi)$, the z-direction would be a preferred direction of displacement. If we want a uniformly distributed direction angle, we have to take a random α angle between 0 and 2π and a random z-coordinate between -1 and $+1$. This random z-coordinate is obtained by the function 1–2 random(0,1) and the angle β is equal to arcos(1–2 random(0,1)).

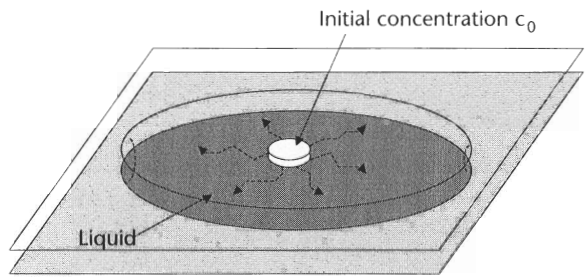

Figure 3.24 Two-dimensional diffusion of tracers originated at a source point.

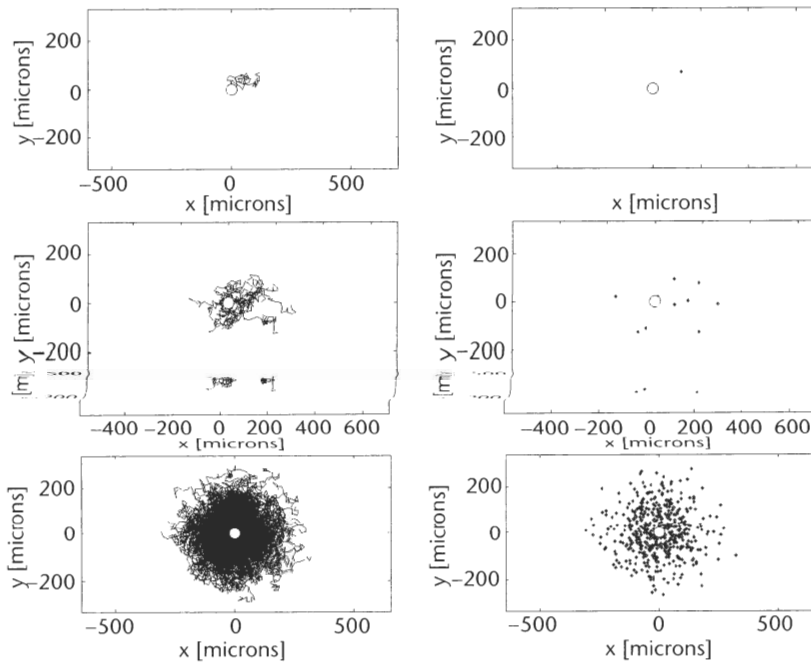

Figure 3.25 Random walk of 10-nm particles originated at the location (0,0). Left, from top to bottom: trajectories for 1, 10, and 500 nanoparticles in a time interval of 50 seconds. Right, from top to bottom: end point of 1, 10, 500 nanoparticles at $t = 50$ seconds.

3.4.2 Diffusion in Confined Volumes: Drug Diffusion in Human Body

3.4.2.1 Introduction

One of the most useful applications of the Monte Carlo method is the diffusion inside a confined domain. It is striking to see how diffusion occurs in very small volumes. In chemistry, there is this example of a solid alloy composed of aluminum with lead inclusions. At a temperature where the lead is molten and the aluminum still solid, one can follow the random walk of the lead molecules inside the aluminum matrix (Figure 3.29) [12].

In biology, there are many examples of diffusion in very confined media: proteins diffuse in cells [13], and macromolecules diffuse in cells' interstitial spaces. Due to its importance, diffusion processes in confined media is the object of many studies, and there is an abundant literature on this topic. We present here an important example in biology: the diffusion in ECSs of cell clusters.

In the biological field, the delivery of drugs in the human body, especially in clusters of cells, is a problem of utmost importance, requiring the knowledge of diffusion in a complex, confined geometry. In this case, there are two different media: the ECS and the cells; these two media are separated by the cell membrane. Diffusion of biological molecules first takes place inside the ECS. After the molecules have penetrated the cells through the cell membranes (which is called uptake), the molecules diffuse inside the cells. In this section, we focus on the *diffusion inside the ECS*.

Because cellular uptake is not immediate, biological cluster of cells may be seen as porous media, where the cells are the *solid grains* and the ECS is the *pores*

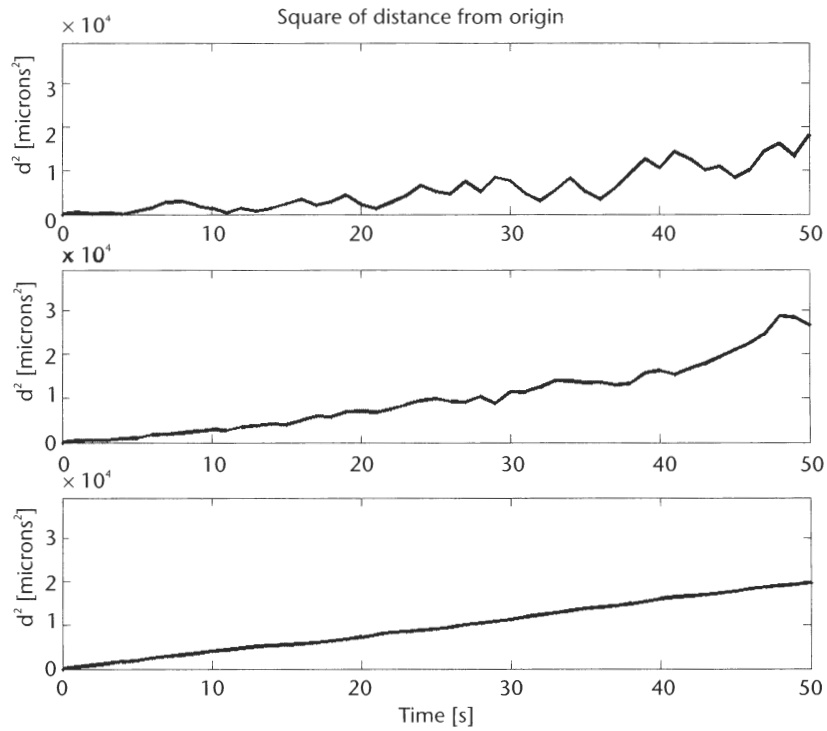

Figure 3.26 Square of average distance of particles versus time. From top to bottom, 1, 10, and 500 nanoparticles. In the third figure at the bottom, the curve is nearly linear, and its slope is approximately $2 \cdot 10^4/50 = 400\ \mu m^2/s$. If we relate this value to the relation $<d^2> = 4Dt$, the value of the slope must be 4D, and we find $D = 10^{-10}\ m^2/s$, which is the input value in the model.

(Figures 3.30 and 3.31). In the particular case of tumoral cells, the extracellular path is called the tumor interstitial matrix (IM) [14].

We will show in the following that diffusion in the ECS is much slower than free diffusion. It is typical to use an apparent (or effective) diffusion coefficient (ADC) to determine the speed of diffusion of drugs in the tumor ECS [15]. Speed of diffusion based on the apparent diffusion coefficient is equal to that of the real diffusion coefficient in the restricted geometry of the ECS. The apparent diffusion coefficient depends on the morphology of the ECS, especially on the tortuosity (Figure 3.32)—ratio of the real distance to the straight line distance between two points—and also to special features of the ECS, like intercleft spaces and constrictions. Real drug delivery time will be determined by adding to the diffusion characteristic time in the ECS the uptake characteristic time (time for the macromolecule to enter the cell) plus the diffusion time inside the cell [13].

Note that it is of great importance in cancer treatment to be able to estimate the value of the apparent diffusion coefficient [16]. If the delivery time is too long—it may reach 48 hours—or if some cells are not delivered, the balance between destruction and multiplication of cancerous cells will be unfavorable. Note also that in some cases, a change of the ADC reflects a change in the cells' shape and arrangement [17], so that an evolution of a disease may be followed.

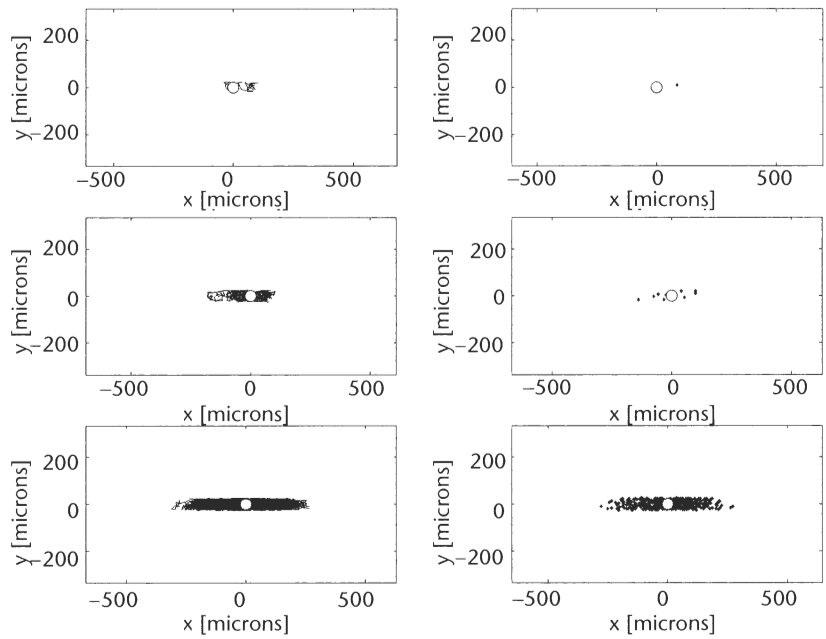

Figure 3.27 Monte Carlo diffusion in a quasi-one-dimensional geometry. Left, from top to bottom: trajectories of 1, 10, and 500 nanoparticles in a time interval of 50 seconds. Right, from top to bottom: end point of the trajectories at $t = 50$ seconds.

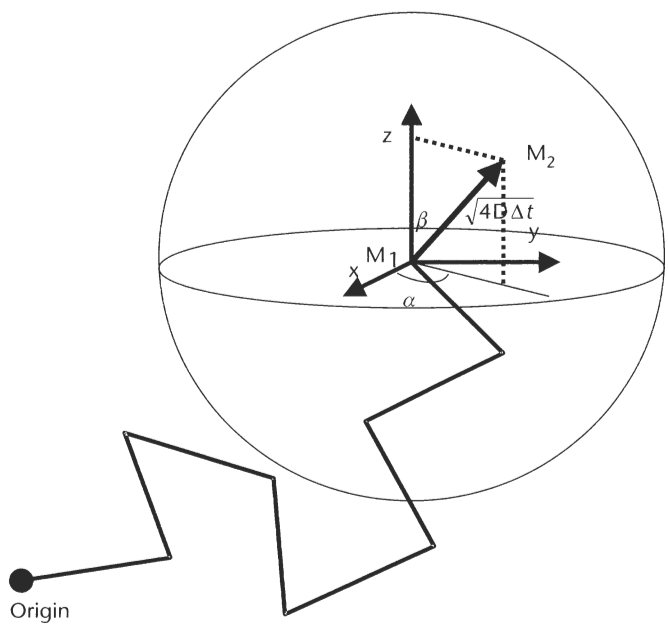

Figure 3.28 Schematic view of the linear motion M_1M_2 during the random walk.

We suppose that the fluid flow in the ECS is negligible in front of the molecular diffusion, so we have to calculate the diffusion of a substance in a very complex

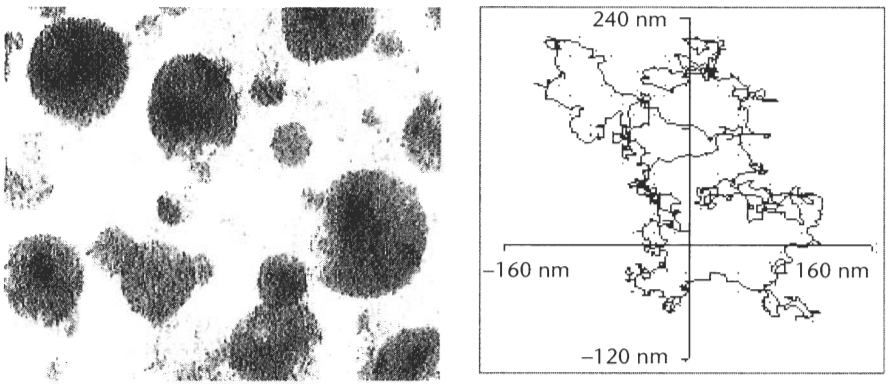

Figure 3.29 Example of very confined diffusion. Lead molecules diffusing inside a aluminum matrix (*From:* [12]. © 2002 Erik Johnson. Reprinted with permission.)

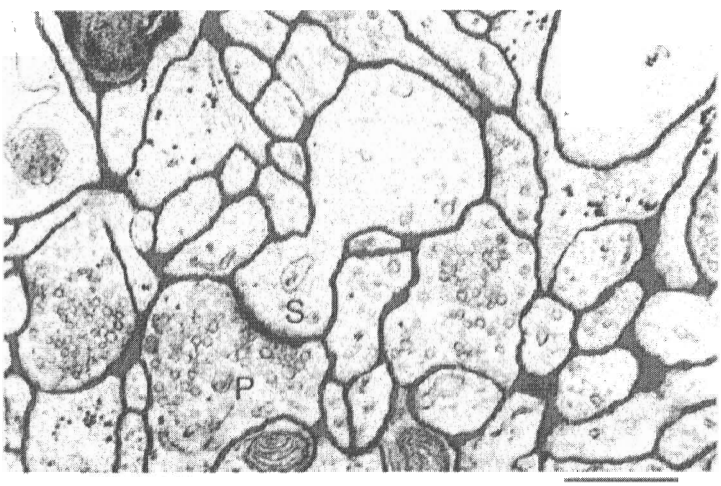

Figure 3.30 Geometry of ECS from [15]. Electromicrograph of small region of rat cortex. The ECS is in dark on the picture. *Lakes*, or intercleft spaces, can be seen at the bottom right where the ECS widens. (*From:* [18]. © 1998 TINS. Reprinted with permission.)

geometry. Different types of numerical approaches have been proposed for regular repetitive patterns like squares and triangles: the homogenization theory [19], which is based on the calculation of the diffusion in a motif and extending the result to the whole domain, and the Monte Carlo method [20] in geometry, where the boundaries are defined by analytical linear functions. At a certain point, it has been thought that regular patterns calculation could be sufficient to approximate an average ADC [21]; however, it is not always the case if the ECS has intercleft spaces or constrictions, particularly if one wants to estimate the local uptake rates [22] or if any change in cell shape and arrangement takes place [19]. So far there have been very few investigations for irregular and disordered clusters, mostly because of the difficulty in describing the geometry [23].

However, recent progress has been made in tackling the problem of diffusion in the ECS of clusters of cells. In the following, we present a two-dimensional numerical approach based on a two-step calculation: first, the calculation of the cells

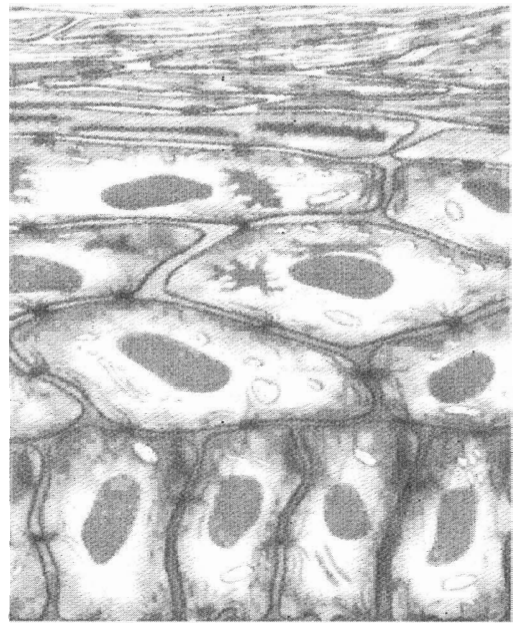

Figure 3.31 Cell arrangement in the human skin from [24]. The shape of the cells is regular, but the anisotropy of the ECS changes from top to bottom. The typical width of the ECS is a few microns. (Courtesy of CEA.)

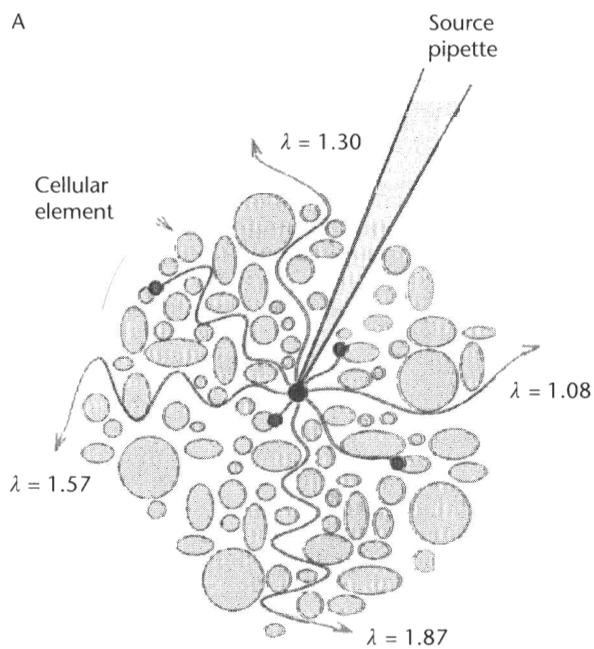

Figure 3.32 Schematic view of the diffusion paths in a porous media, depending on the tortuosity.

boundaries; second, a Monte Carlo numerical scheme for the diffusion in the ECS morphology defined at the preceding step.

3.4.2.2 Cell Boundaries

First, cells arrangement may be mimicked: cells rearrange inside the boundaries of the cell cluster in a function of constraints, like the surface tension of the membranes and their volume (depending on the growth or the shrinking of cells). A numerical software like the Surface Evolver [25] (see Chapter 2) is well adapted to calculate the morphology of the cell cluster. In order to describe a cell cluster morphology, a given set of points (vertices), segments (edges) delimiting the initial cells, is introduced in the Evolver numerical program. Depending on line (surface) tensions and cell volumes, the shape of the cells evolves until convergence to a minimum energy arrangement, mimicking real cell arrangement, is reached. It is assumed here that cell membranes behave similarly to an interface with surface tension. The initial edges are then refined and deformed depending on the specified constraints. A calculated arrangement of cells mimicking a real cluster of cells has been plotted in the Figure 3.33.

In the Evolver approach, the computational nodes are located on the cells' edges and are referenced by their coordinates (x, y) and by the corresponding edge number. Besides, each cell is referenced by its oriented edges. In order to prepare step 2, all of this information is memorized and stored.

3.4.2.3 Monte Carlo Numerical Scheme

Particles—or macromolecules—are initially placed in a central microregion, simulating the injection point at the tip of the microneedle. Diffusion is then simulated by following the particles executing random walks inside the ECS. In a two-dimensional system, the displacement $(\Delta x, \Delta y)$ of any particle in the time step Δt is given by the relations

$$\Delta x = \sqrt{4D\Delta t}\cos(\alpha)$$
$$\Delta y = \sqrt{4D\Delta t}\sin(\alpha)$$
$$\alpha = random(0,2\pi)$$

where D is the *free* diffusion coefficient, given by Einstein's law

$$D = \frac{k_B T}{6\pi\eta R_H}$$

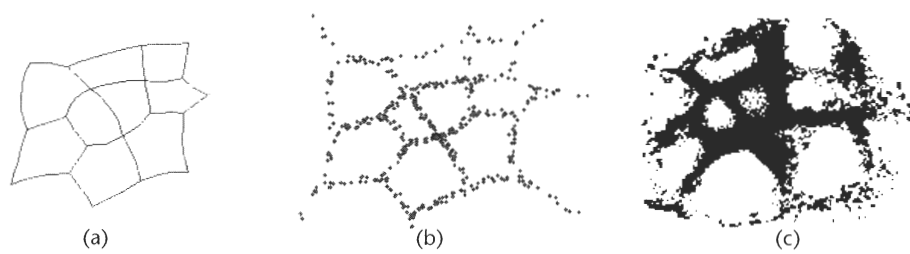

Figure 3.33 (a) Cell arrangement is calculated with the Evolver numerical program; (b) cell cluster morphology is enlightened by the calculated location of pharmaceutical molecules after they have diffused in the ECS; and (c) real cell cluster is observed by fluorescence imaging.

where k_B is the Boltzman constant ($1.38 \cdot 10^{-23}$ J/K), T is the temperature (K), η is the dynamic viscosity of the carrier fluid, and R_H is the hydraulic radius of the particle.

3.4.2.4 Uniform and Narrow ECS

Suppose first that the width of the ECS is approximately constant (as in Figure 3.33). The cell edges defined in the preceding step are widened to the desired width to define a real ECS. Particles location inside the cluster is permanently tracked, and the particles are not allowed to cross solid (cell) boundaries. The random walk of particles may then be confined inside the ECS, as shown in Figure 3.34. If the time allowed for the calculation is sufficiently large, the ECS is explored by the diffusing particles, as shown in Figure 3.35.

In a porous media, the distance between two points may be defined as the length of the shortest line in the fluid domain between two points (Figure 3.36), and tortuosity is then defined as the ratio between the distance in the liquid and the straight line distance.

It may be theoretically shown [19] that for any two-dimensional regular isotropic lattice of convex cells, tortuosity has a unique value

$$\tau = \sqrt{2} \tag{3.50}$$

and for three-dimensional lattices, the value of the tortuosity is

$$\tau = \sqrt{3} \tag{3.51}$$

It is relatively easy to be convinced of the validity of (3.50) and (3.51). Because the media is isotropic, we can estimate the tortuosity on a diagonal direction (Figure 3.37). We can approximate the length L_{AB} by a pixel discretization: By projection on the horizontal and vertical axis, assuming a discretization $\Delta x = \Delta y$, we obtain

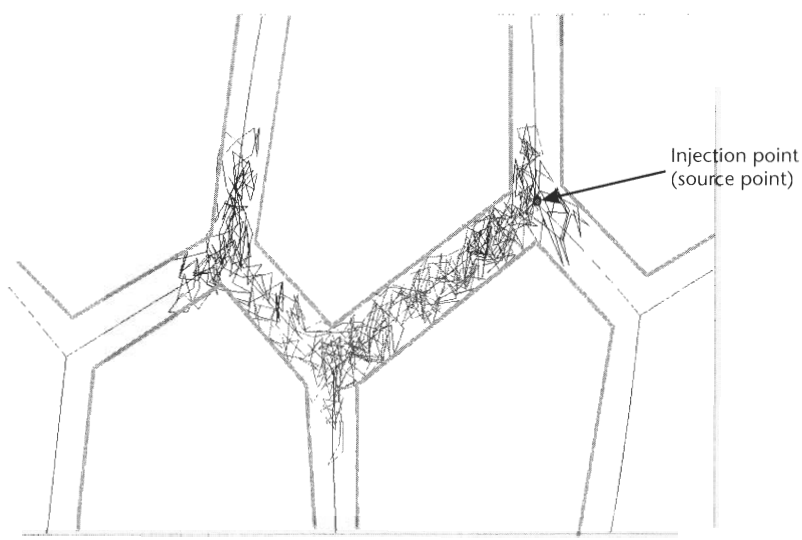

Figure 3.34 Random walk of two particles inside an ECS calculated by a Monte Carlo method and constrained by ECS boundaries.

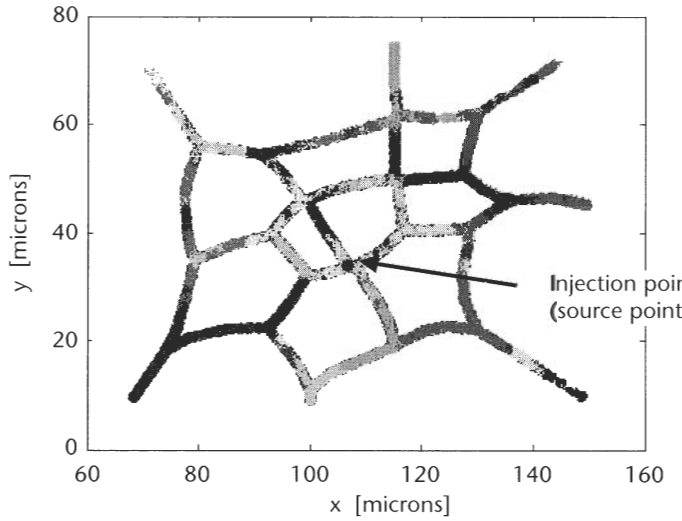

Figure 3.35 Random walk of 200 particles inside the ECS of the cluster.

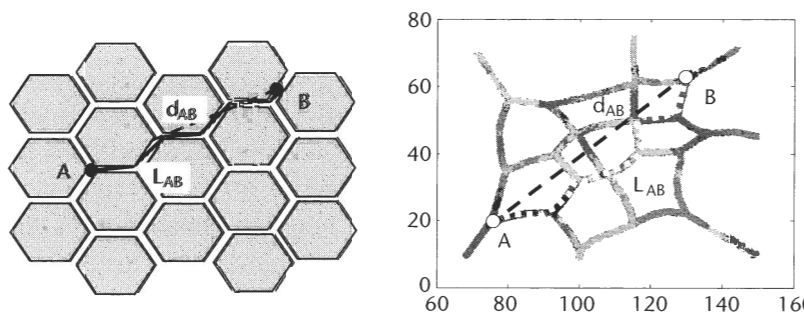

Figure 3.36 Definition of tortuosity in regular and irregular lattices. The tortuosity τ is equal to the ratio L_{AB}/d_{AB}; in a free media, τ =1.

$$L_{AB} = n\Delta x + n\Delta y = 2n\Delta x$$

On the other hand, the Pythagore relation is

$$d_{AB}^2 = (n\Delta x)^2 + (n\Delta y)^2 = 2n^2\Delta x^2$$

Combining the two preceding equations yields

$$\tau^2 = \frac{L_{AB}^2}{d_{AB}^2} = \frac{4n^2\Delta x^2}{2n^2\Delta x^2} = 2$$

Finally,

$$\tau = \frac{L_{AB}}{d_{AB}} = \sqrt{2}$$

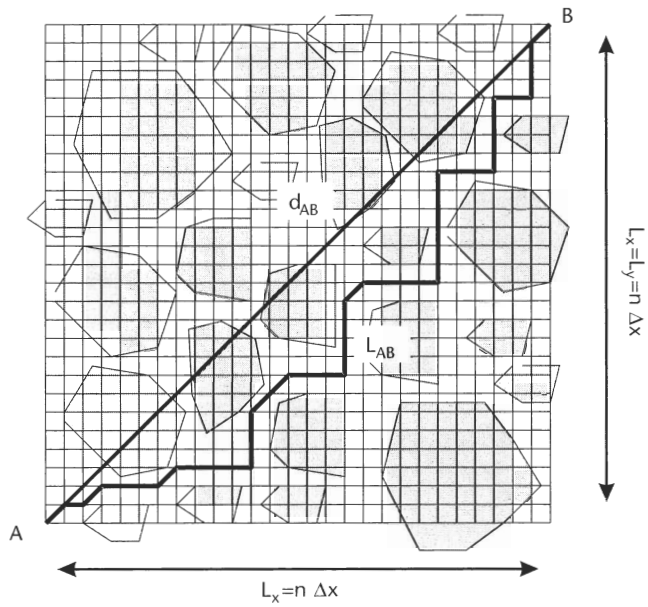

Figure 3.37 Estimation of the tortuosity in the case of convex, isotropic porous media.

The same reasoning also applies to the three-dimensional case.

It has been also shown that there is a very simple relation between the effective and the free diffusion coefficient involving the tortuosity

$$\frac{D_{eff}}{D} = \frac{1}{\tau^2} \tag{3.52}$$

Thus, if the width of the ECS is narrow and remains uniformly constant in the two-dimensional cluster, the value of the effective diffusion coefficient is half that of the free diffusion coefficient

$$\frac{D_{eff}}{D} = \frac{1}{2}$$

Assuming the same conditions for the ECS (isotropy and convexity), the Monte Carlo numerical model shows that (3.50) and (3.52) also apply for any isotropic cluster of irregular cells. Figure 3.38 shows the location of the diffusing particles initially starting from the injection point after a time interval of 15 seconds ($D = 10^{-10}$ m^2/s).

Let's introduce the normalized diffusion length β by

$$\beta = \frac{L}{\sqrt{4Dt}} \tag{3.53}$$

where L is obtained by averaging the distance of each particle between their location at time t and at time $t = 0$.

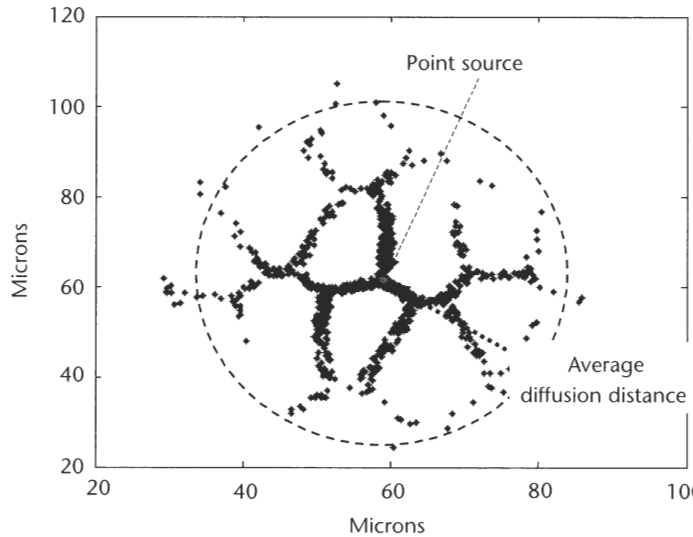

Figure 3.38 Diffusion distance from point source in an isotropic cell cluster.

In Figure 3.39, we plotted the normalized diffusion length versus time for different cluster morphologies: ordered (square and hexagonal cells) and disordered, with narrow ECS. A narrow ECS is defined here by a constant width less than one-tenth of the average size of the cells but larger than about three times the mean free path of the particles.

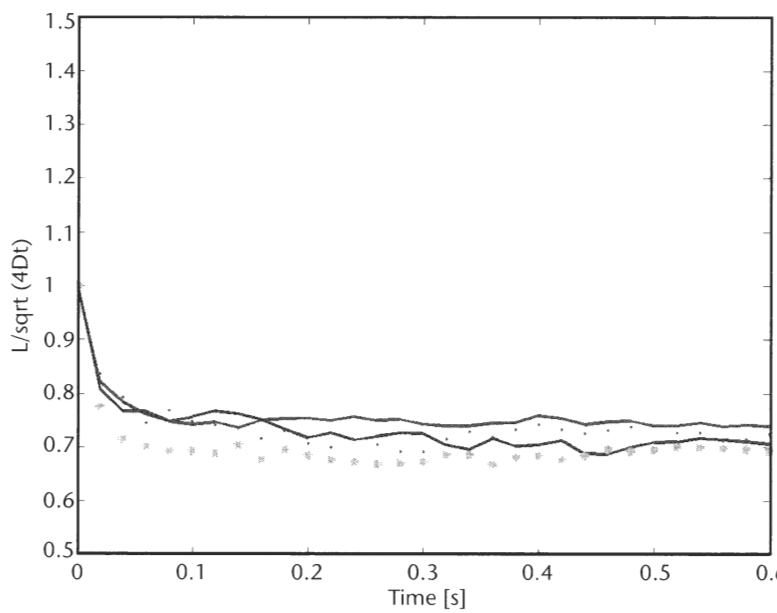

Figure 3.39 Normalized diffusion length versus time for different cluster morphologies (ordered and disordered) with narrow ECSs. The curves are similar to the experimental results of de Sousa et al. [26].

At very small times, the diffusing particles execute random walk inside a small region of the ECS where the particles are initially placed, so that the value of β is that of free diffusion: $\beta = 1$ at $t = 0$. After a short time, the particles have explored all of the available initial space and start diffusing inside the ECS. They are now constrained inside the ECS by the cells' boundaries, and β reaches a nearly constant value. The numerical results of Figure 3.39 are very similar to that of de Sousa et al. [26], obtained experimentally for regular triangle and square lattices.

The asymptotic value of β is 0.7, thus

$$\beta = \frac{L}{\sqrt{4Dt}} \approx 0.7 \approx \frac{1}{\sqrt{2}} \tag{3.54}$$

By definition, the apparent diffusion coefficient satisfies

$$\frac{L}{\sqrt{4D_{eff}t}} \approx 1 \tag{3.55}$$

From (3.54) and (3.55), we find the relation

$$\frac{D_{eff}}{D} = \beta^2 = \frac{1}{\tau^2} \approx \frac{1}{2} \tag{3.56}$$

leading to the value $\tau = \sqrt{2}$.

3.4.2.5 Intercleft Spaces and Channel Restrictions

Real ECSs in the human body are often more complex than that of a uniformly narrow gap between the cells, which we analyzed in the preceding section (see Figure 3.30). Very often, the spacing of the cells' lattice is not uniform, and there are intercleft spaces. It is shown that diffusion speed may be reduced by entrapment when the dimensions of the residual spaces are large and the connecting exits are sufficiently small. By "sufficiently small," we mean that the mean free path of the particle inside the carrier fluid is of the order of the cross dimensions of the ECS.

An idealized example is that of a cluster of round cells. If the dimension of the gaps between the cells is decreased, the apparent diffusion coefficient becomes smaller than the value predicted by (3.6). In the case defined in Figure 3.40, we obtain $\frac{D_{eff}}{D} \approx \frac{1}{4}$.

A limiting case is that of a gap width of the order of the mean free path of the particle, in such a case that the particles are trapped inside the intercleft space. In such a case, the relevant theory is the *percolation theory*, and there have been considerable efforts in this domain for biological applications.

3.4.2.6 Discussion

We have modeled the diffusion of biochemical species in a cluster of cells by a three-step algorithm: (1) generation of a cluster arrangement using the Evolver

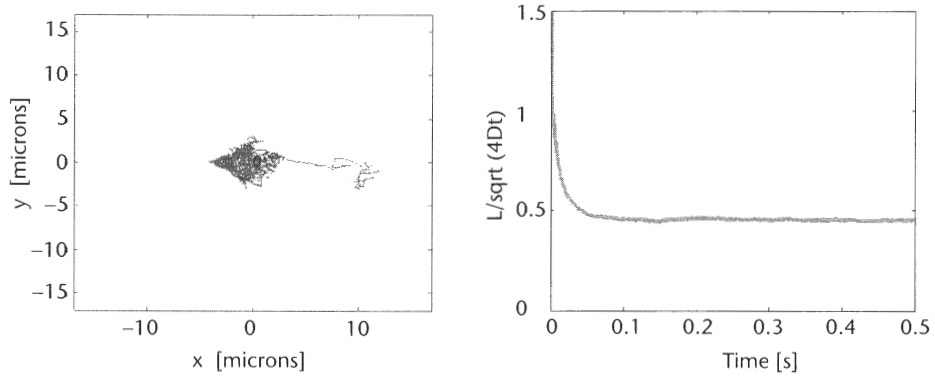

Figure 3.40 Normalized diffusion length versus time for a cluster of round cells with small gaps.

numerical software, (2) Monte Carlo random walk of the diffusing species, and (3) particle tracking to constrain the diffusing species inside the ECS.

The results of the model show that the ratio between the apparent diffusion coefficient and the free diffusion coefficient in dense cell clusters with small ECS is always the same, no matter what the morphology of the cluster (ordered or disordered) is. In a two-dimensional cluster

$$\frac{D_{eff}}{D} = \frac{1}{\tau^2} \approx \frac{1}{2}$$

where τ is the tortuosity of the porous media. However the situation is much more complex in the ECS of irregular and anisotropic clusters of cells, especially if there exists intercleft spaces. There are two cases where speed of diffusion can be considerably reduced: first, by particle entrapment in the intercleft spaces of the ECS, and second, in the case of an anisotropic medium, diffusion in the direction perpendicular to the preferred direction of the medium is delayed.

3.5 Conclusion

Diffusion is probably the main phenomenon concerning micro- and nanoparticles and target macromolecules in biotechnological applications. Estimation of diffusion time may be performed by solving the partial differential equation for the diffusion of concentration or by a discrete approach. The advantage of the *continuum* approach is the availability of numerical software—finite element method is recommended because it adapts best to the shape of the boundaries—and the relative fast computational time—at least in a two-dimensional case. A discrete approach—like the Monte Carlo method—is perhaps more demonstrative because it mimics the behavior of the particles and is well adapted to very complicated geometries. The drawback of the method is the computational time.

For the technological applications, diffusion is at the same time advantageous and not: for example, it takes advantage of the Brownian motion to make molecules recognize each other leading to the desired hybridization; on the other side, diffusion

may disperse the target molecules or mix these molecules with other undesirable molecules. The art of the design of biotechnological components resides in part in the clever uses of molecular diffusion.

References

[1] http://scienceworld.wolfram.com/physics/BrownianMotion.html.

[2] Tabeling, P., *Introduction à la Microfluidique*, Paris: Belin, 2003.

[3] Hiementz, P. C., and R. Rajagopalan, *Principles of Colloid and Surface Chemistry*, New York: Marcel Dekker, 1997.

[4] Crank, J., *The Mathematics of Diffusion*, 2nd ed., Oxford, England: Oxford University Press, 1975.

[5] Faucheux, L. P., and A. J. Libchaber, "Confined Brownian Motion," *Physical Review E.*, Vol. 49, No. 6, 1994.

[6] Press, W. H., et al., *Numerical Recipes*, Cambridge, England: Cambridge University Press, 1987.

[7] Berthier, J., and F. Chatelain, "Dimensioning Simultaneous Polymerase Chain Reactions in Capillary Tubes," *Proc. of 2005 FEMLAB Conference*, Paris, France, November 15, 2005.

[8] Buckingham, E., "On Physically Similar Systems: Illustrations of the Use of Dimensional Equations," *Phys. Rev.*, Vol. 4, 1914, pp. 345–376.

[9] FEMLAB reference manual. Stockholm: COMSOL AB, http://www.comsol.com.

[10] de Gennes, G., "Polymers at an Interface: A Simplified View," *Adv. Colloid Interface Sci.*, Vol. 27, No. 5, 1987, pp. 189–209.

[11] MATLAB software manual: http://www.mathworks.com.

[12] Johnson, E., et al., "Nanoscale Lead-Tin Inclusions in Aluminium," *J. Electron Microscopy*, Vol. 51, 2002, pp. S201–S209.

[13] Pollack, G. H., *Cells, Gels and the Engines of Life*, Seattle, WA: Ebner and Sons, 2001.

[14] Rumanian, S., et al., "Diffusion and Convection in Collagen Gels: Implications for Transport in the Tumor Interstitium," *Biophys. J.*, Vol. 83, 2002, pp. 1650–1660.

[15] Lankelma, J., et al., "A Mathematical Model of Drug Transport in Human Breast Cancer," *Microvascular Research*, Vol. 59, 2000, pp. 149–161.

[16] El-Kareh, A. W., S. L. Braunstein, and T. W. Secomb, "Effect of Cell Arrangement and Interstitial Volume Fraction on the Diffusivity of Monoclonal Antibodies in Tissue," *Biophys. J.*, Vol. 64, 1993, pp. 1638–1646.

[17] Herneth, A. M., S. Guccione, and M. Bednarski, "Apparent Diffusion Coefficient: A Quantitative Parameter for In Vivo Tumor Characterization," *European J. of Radiology*, Vol. 45, 2003, pp. 208–213.

[18] Nicholson, C., and E. Sykova, "Extracellular Space Structure Revealed by Diffusion Analysis," *TINS*, Vol. 21 No. 5, 1998, pp. 207–215.

[19] Chen, K. C., and C. Nicholson, "Changes in Brain Cell Shape Create Residual Extracellular Space Volume and Explain Tortuosity Behavior During Osmotic Challenge," *Proc. Natl. Acad. Sci. USA*, Vol. 97, No. 15, 1999, pp. 8306–8311.

[20] Saxton, M. J., "Lateral Diffusion in an Archipelago, the Effect of Mobile Obstacles," *Biophys. J.*, Vol. 52, 1987, pp. 989–997.

[21] Blum, J. J., et al., "Effect of Cytoskeletal Geometry on Intracellular Diffusion," *Biophys. J.*, Vol. 56, 1989, pp. 995–1005.

[22] Szafer, A., et al., "Theoretical Model for Water Diffusion in Tissues," *Magnetics Resonance in Medicine*, Vol. 33, No. 5, 1995, pp. 697–712.

[23] Berthier, J., F. Rivera, and P. Caillat, "Numerical Modeling of Diffusion in Extracellular Space of Biological Cell Clusters and Tumors," *Nanotech 2004*, Boston, MA, March 7–11, 2004.

[24] Martin, M., "Conséquences D'une Irradiation Ionisante Sur la Peau Humaine," *Clefs CEA*, Vol. 48, 2003, pp. 53–55.

[25] Brakke, K. A., "The Surface Evolver," *Experimental Mathematics*, Vol. 1, No. 2, 1992, pp. 141–165.

[26] de Sousa, P. L., D. Abergel, and J.-Y. Lallemand, "Experimental Time Saving in NMR Measurement of Time Dependent Diffusion Coefficients," *Chemical Physics Letters*, Vol. 342, 2001.